29th AIAA Applied Aerodynamics Conference
27 - 30 June 2011, Honolulu, Hawaii

AIAA 2011-3810

Performance of an Airfoil with a Power-saving, Tab-assisted Flap System

Joseph R. Bottalla[1] and Michael B. Bragg[2]
University of Illinois at Urbana-Champaign, Urbana, IL 61801

and

James J. Sheahan Jr.[3] and Chad M. Winkler[4]
The Boeing Company, Hazelwood, Missouri 63042

This study investigated the feasibility of reducing control surface input power with the use of a tab-assisted flap. Wind tunnel tests were conducted at the University of Illinois at Urbana-Champaign on a NACA 3415 airfoil model with a flap including an active trim tab. Measurements were taken for two configurations: a baseline fixed tab case where tab deflection was zero and a tabbed case where multiple flap and tab angle combinations were tested. Hinge moment measurements were taken for both the flap and tab and confirmed the ability to actuate and hold the flap with the trim tab. Lift, drag and moment measurements along with surface pressures were acquired to aid in the analysis of the concept. Results are presented for hinge moment reductions along with lift and drag penalties. An additional study on several flap deflection scenarios was conducted to assess approximate work savings. Computational studies were also performed and compared well to experimental values except when large regions of unsteady separated flow were present.

Nomenclature

α	angle of attack
δt	tab deflection angle
δf	flap deflection angle
C_d	drag coefficient
C_h	hinge moment coefficient
C_l	lift coefficient
$C_{l\,max}$	maximum lift coefficient
C_m	quarter-chord pitching moment coefficient
C_p	pressure coefficient
M	Mach number
Re	freestream Reynolds number, based on the airfoil chord length
x/c	chordwise location

I. Introduction

Flight control systems for Next Generation Air Vehicles will require the implementation of new technologies. With thinner wings requiring installation in a much smaller volume, supercritical airfoil shapes requiring higher holding loads resulting in thermal issues, and the migration towards more electric aircraft, a flight control actuation system is needed that reduces size, weight, and power/thermal requirements.

With the ever increasing need for larger control surfaces and higher powered actuators for flight controls, supply power sources have grown and heat rejection has risen dramatically. Aircraft such as the blended-wing body

[1] Graduate Research Assistant, Department of Aerospace Engineering, Member AIAA.
[2] Professor of Aerospace Engineering, Executive Associate Dean for Academic Affairs, Fellow AIAA.
[3] Associate Technical Fellow, Boeing Research and Technology, Member AIAA
[4] Associate Technical Fellow, Boeing Research and Technology, Member AIAA

will have control surfaces up to five feet in chordwise extent. Actuating such a surface necessitates large amounts of power to supply the larger actuators. To reduce the thermal impact and power requirements for the flight controls, an alternate approach for flight control method needs to be developed. Such alternatives include fluidic actuation, wing warping, and multiple joint flight control surfaces.

The effects of tabs on other surfaces have been studied since NACA research such as the investigation by Holtzclaw and Crane,[1] in 1944, where wind-tunnel tests were performed on a NACA (66)2-216 airfoil model with 20%-chord tabbed ailerons. These tests looked at the general effects on lift and hinge moments for two different airfoil profiles for application with fixed tabs. Even earlier in 1936, Jones and Nerken[2] completed a study on the hinge moment reduction with ground-adjustable fixed tabs for ailerons and found a deflection that trims the ailerons upward was most beneficial. Two years later, Soulé and Hootman[3] conducted the same experiment but with a flight test program. These tabs were installed and ground-adjusted to several different downward deflections. While the tabs were found to reduce stick forces, it was left to the discretion of the pilots themselves to determine the relative control forces. The research determined that fixed tabs were impractical for active reduction of hinge moments.

Another NACA study by Harris[4] surveyed the effects of different geometries of tabs on each of the typical aircraft control surfaces: aileron, elevator and rudder. The tab in this case was used in two different methods, trimming or active control, referred to as a servo-control tab where the tab is the active control surface. Trimming was also implemented by either direct control, as typically used today on elevators, or by ground fixing. Data were taken for hinge moment reductions as well as the effect on the normal force coefficient, from which the lift and drag penalties could be found. Results indicated a large potential savings for each control surface but were limited to smaller deflections.

Using a very similar experimental method as this research, Ansell[5] performed wind-tunnel experimentation with a NACA 3415 airfoil model to assess the feasibility of providing stall warning by utilizing flap and control surface hinge moments for models with and without contamination. A fixed tab was later added to find its effect on the unsteady hinge moment.[6] Again, this was a fixed tab but provided valuable hinge moment data.

For this experiment, the mode of operation is simple - the tab is moved to a fully deflected position that results in air loads that provide actuation for the primary flap system. When the surface reaches its commanded position the tab returns to its neutral position resulting in full surface aerodynamic authority while using a fraction of the power that direct flap actuation would have required. Based on the current desire to produce more electric aircraft this system was developed using Electro-Mechanical Actuators (EMAs). Using math models of the flight control system a simulation was performed of the flight surface motion and actuator. With this configuration the tab can be held stationery and used as part of the flight control surface, when full authority is required. Based on these simulations, the tab and primary surface working together in this way results in reducing the power required by as much as 90% during specific portions of the duty cycle and 50% over the flight duration.

Based on these results, computational fluid dynamic (CFD) analysis and wind tunnel testing were required to validate the findings of the simulations. The approach for this experimental/computational analysis was simplified to look at the effects of a tab deflection on the aerodynamic performance and hinge moment under a fixed flap deflection. This paper will present the data from both the experimental and computational investigations and studies on the power-savings capability of using a tab for assisting a flap. It will also address the tradeoffs in potential drag increase and loss of lift. Future experiments will address the mode of operation described above.

II. Experimental Methodology

All of the wind-tunnel experiments reported here were conducted at the Aerodynamics Research Laboratory at the University of Illinois at Urbana-Champaign. The wind tunnel is a subsonic, open return tunnel with a maximum speed of 235 ft/sec. and a rectangular test section measuring approximately 3-ft by 4-ft. The airfoil used in the investigation was a NACA 3415 with a simple flap: with and without a tab. The model has a 1.5-ft chord with a 25% chord flap and a 25% flap chord tab. The model spanned the height of the test section from tunnel floor to ceiling.

The model was installed on a three-component force balance, located below the tunnel test section, capable of measuring lift, drag and pitching moment. Both the tab and flap were actuated using two link arms attached to linear traverses. Linear compression/tension load cells were integrated into the link arms to measure the hinge moments. Figure 1 below illustrates the flap/tab linkage systems. In addition, all three elements of the model were equipped with surface pressure taps near the midspan location.

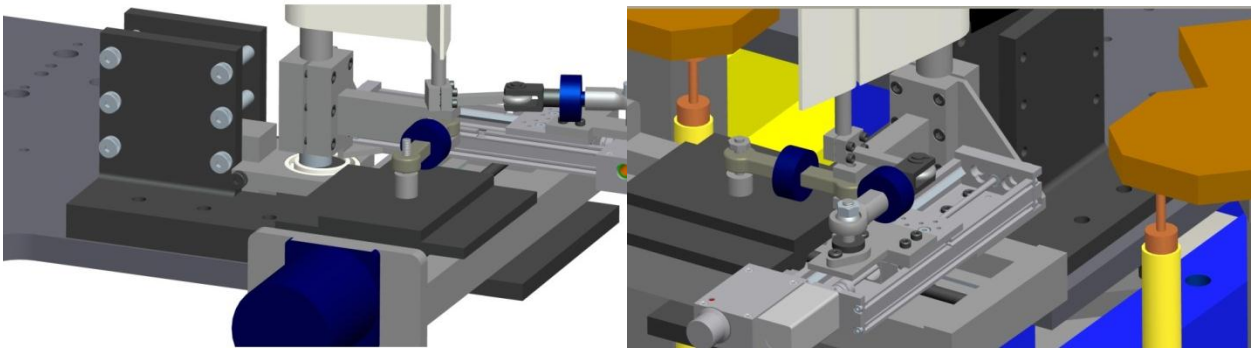

a) b)

Figure 1. Drawings of a) flap and b) tab linkage systems installed below wind tunnel test section.

A traversable wake rake located roughly 1.25 chord lengths behind the model was used to measure the drag. The pressures from the wake rake and the model were measured with an electronically-scanned pressure (ESP) system. A schematic of the experimental setup is shown below in Fig. 2. A top view of the airfoil model with model, flap and tab moment and rotation centers dimensioned follows in Fig. 3.

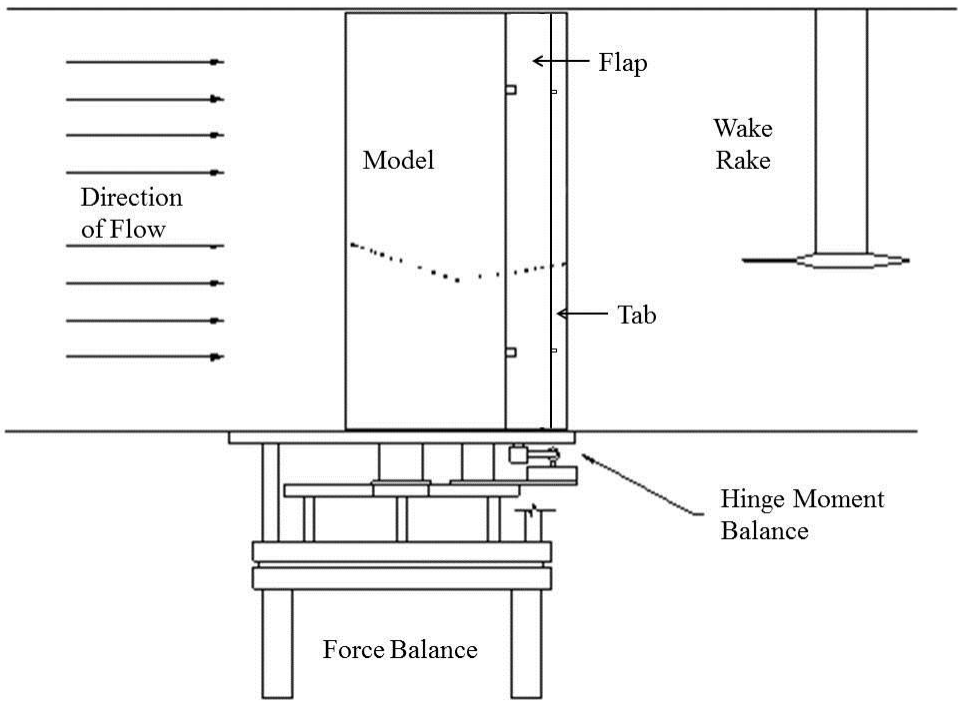

Figure 2. Schematic of experimental setup, adapted from Lee.[7]

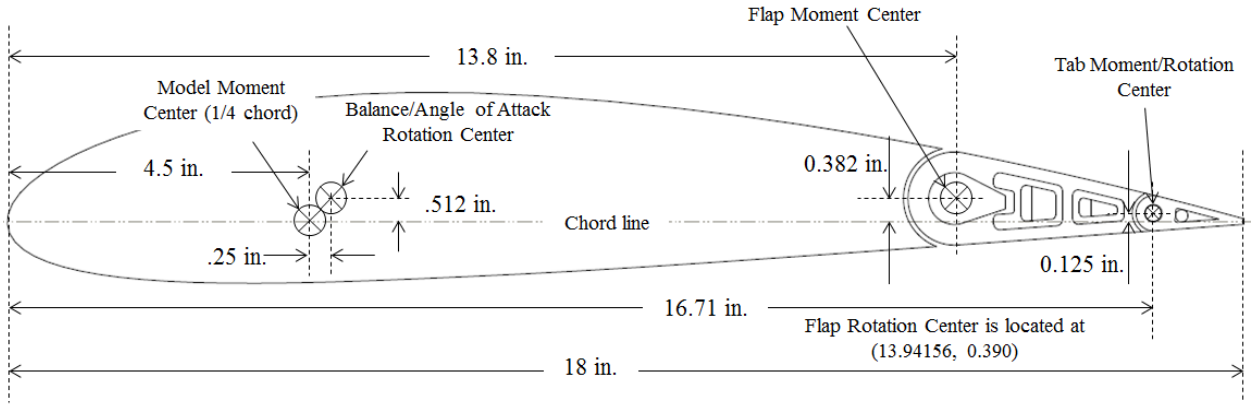

Figure 3. Top-view schematic of airfoil model with moment and rotation centers.

Both the surface pressure and force balance measurements were used to calculate the lift coefficient and the pitching moment about the quarter-chord. Due to the lack of sufficient pressure taps on the flap and tab, the data for C_l and C_m presented in this paper were taken from the force balance. The surface pressure measurements were used for pressure coefficient distribution plots to analyze flow phenomena. The drag coefficient was calculated using the wake pressure data and standard momentum-deficit methods. All of the data, including angle of attack, were corrected for wall-interference using methods by Rae and Pope.[8]

For both the baseline and tabbed cases, angles of attack from -6 deg. to stall by 2 deg. increments with 1 deg. increments near stall. Flap angles of ±30, ±20, ±10, ±5 and 0 deg. were tested with tab deflections of ±60, ±45, ±30, ±15 and 0 deg. and additional deflections were tested for each flap angle in the region of zero flap hinge moment for the tabbed cases. Extra runs examined the possible hysteresis in measured forces and moments due to flap deflection and angle of attack. All data were taken at Re = 1.8 million and M = 0.18.

Surface-oil flow visualization was used to examine a few of the cases where further information on the flowfield was desired. These runs were made at the same Mach number and Reynolds number as the rest of the experiment.

III. Computational Methodology

Computations of the NACA 3415 in the UIUC tunnel were accomplished using the BCFD code. The BCFD code is a general geometry and general purpose Euler and Navier-Stokes flow solver. Presently, BCFD is capable of solving multi-dimensional flowfields using both mixed-element unstructured grids and/or convectional structured (patched and overlapping) grids. The core structured grid solver began as McDonnell-Douglas's NASTD[9] code which later became the flow solver of the NPARC Alliance (a collaboration between The Boeing Company, Arnold Engineering Development Center, and NASA Glenn Research Center) and the name was changed to WIND.[10] With the addition of the unstructured grid capability, Boeing created the BCFD code[11] to protect proprietary technology and has since worked extensively to improve numerical accuracy and modeling on unstructured meshes.

BCFD has a mature and extensive library of boundary conditions applicable to both external aerodynamic and internal propulsion applications. A mature zone coupling technique ensures continuity of the solution across zone boundaries to facilitate distributed computing. Numerous flux functions are available for the inviscid spatial operator including the Roe, HLLE, and Rusanov algorithms for both first and second-order accuracy on unstructured meshes. BCFD is capable of both steady-state and time-accurate analysis. For unsteady flowfields the time-accurate capability is exercised and provides global second-order temporal accuracy using a dual-time/Global Newton algorithm. BCFD's unstructured RANS equation set is closed by either the Spalart-Allmaras (S-A) one-equation turbulence model[12] or Menter's two-equation Shear-Stress Transport model.[13]

BCFD has been validated in numerous relevant cases, most recently and relevantly in the 4th AIAA Drag Prediction Workshop.[14] For unsteady simulations, BCFD has been validated in isotropic turbulence, stalled airfoils, and aero-optic configurations[15] using the Delayed Detached Eddy Simulation model, among others.[16] Additionally, BCFD has a low-dissipation scheme specifically designed for DES simulations on unstructured grids.

With the exception of the time-accurate runs, all grids were two-dimensional. Near-wall spacing was set to 0.0001 in., which implies the first grid point is half that distance to the wall due to the cell-centered nature of the

code. Grids were generated with MADCAP and AFLR. Typical two-dimensional grid sizes were approximately 180,000 cells. The SST turbulence model was used for the steady-state simulations, with fully turbulent boundary layers. The unsteady simulations used the S-A based DDES model with bounded central differencing on the convective terms to reduce dissipation.

A sample grid of the α = 17 deg., δf = -30 deg. and δt = -30 deg. case is shown in Fig. 4. Note that the tunnel walls are modeled as viscous surfaces and the gaps between the wing/flap/tab are also modeled.

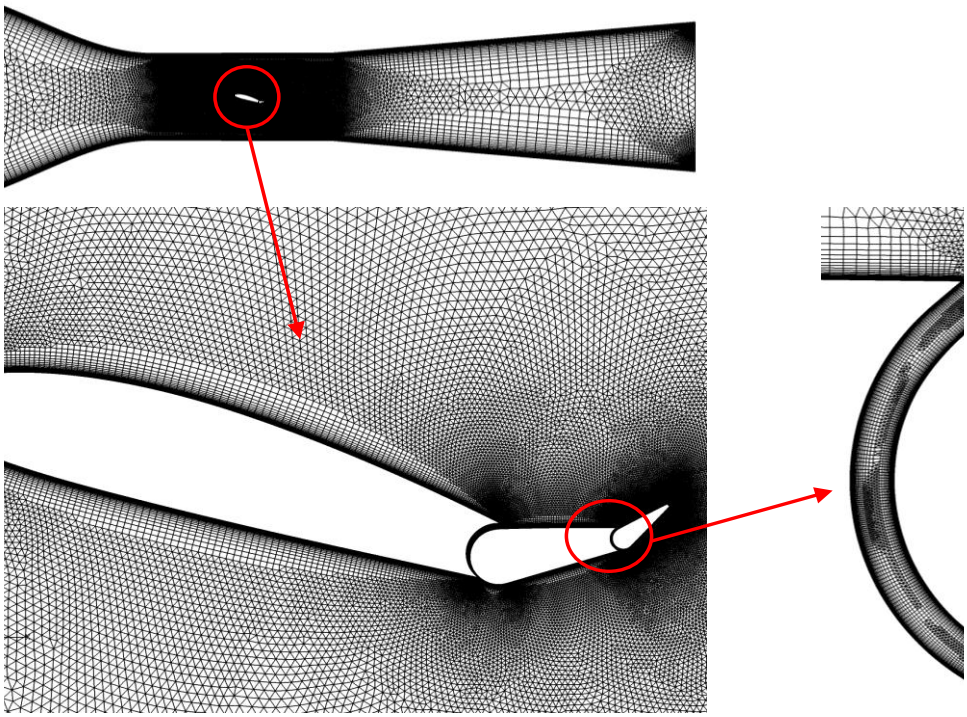

Figure 4. View of computational grid.

For each 2-D configuration, the following angles of attack were simulated: 0, 2, 4, 6, 8, 10, 12, 14, 15, 16, and 17 deg. This gave 121 steady-state solutions. Mass flow was adjusted via backpressure to maintain a Mach number of 0.18 at the start of the test section. The run matrix for steady-state simulations is located to the right in Table 1.

For the unsteady CFD, the δf = -30 deg. and δt = -30 deg. case was run for two angles of attack: α = 0 and 10 deg. Grids were 99 cells in the spanwise direction, and had a span size equal to the tunnel dimension. Grids were extruded two-dimensional meshes using AFLR2D. The spanwise ends of the tunnel were treated as inviscid, whereas the top/bottom of the tunnel was viscous. The time-step was chosen to be 7.39E-5 seconds, which corresponds to 100 time steps per convective turn-over based on a chord of 18 in. and *Re* =1.8 million. Solutions were saved every five time-steps for 70 turn-over times.

Table 1. CFD steady-state run matrix

δf (deg.)	*δt (deg.)*
0	0
10	0
20	0
30	0
-10	0
-20	0
-30	0
-30	-30
0	-5
10	-30
-10	30

IV. Results and Discussion

Results for the baseline case are presented first for comparison purposes and to display the effect of a 25% simple flap on the NACA 3415 model. Next, the data for the tabbed cases are presented and compared against the baseline (δt = 0 deg.) case to study the hinge moment differences between the two methods as well as the effect on the lift and drag that results from using a tab for flap assistance. Computational fluid dynamics results will also be validated using the experimental results and provide additional insight on the hinge moment results and on the flowfield for diagnosis of the important flow phenomena.

A. Baseline Cases

For insight on the flap effectiveness for the NACA 3415 model, data for the lift, hinge moment, drag and pitching moment coefficients are shown in Fig. 5.

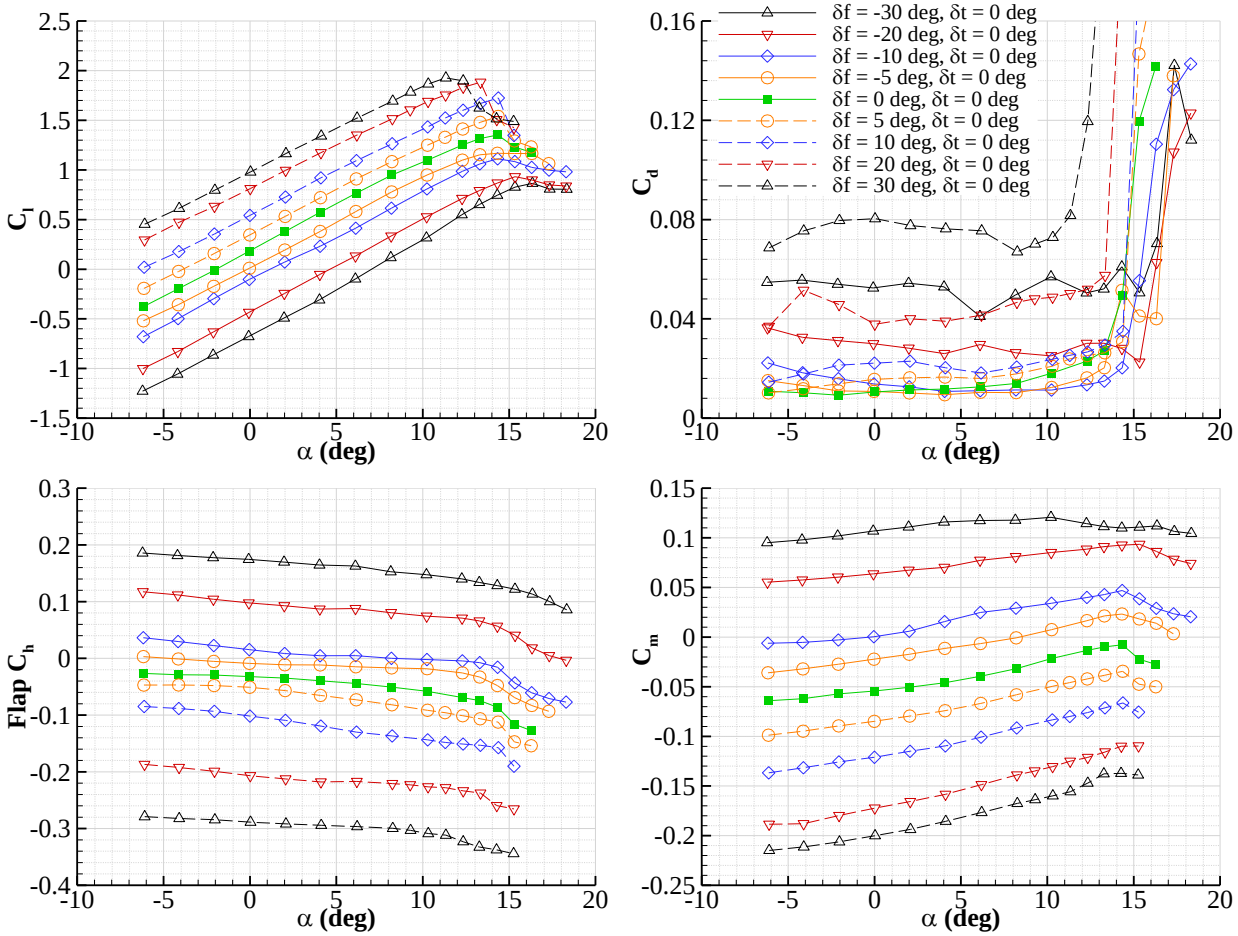

Figure 5. NACA 3415 performance over range of flap deflections with δt = 0 deg.

In Fig. 5, typical flapped-airfoil behavior was seen where the lift curves for all flap deflections remain relatively constant while the angle of attack for maximum lift coefficient decreases for increasing flap angle. The stall becomes sharper for positive deflections while becoming flatter for larger negative deflections suggesting changes in stalling process.

The hinge moment coefficient data for the flap also exhibits classic behavior but with a slight non-linearity in the slope for 0 and ± 5 deg. flap angles. The drag coefficient data illustrate the large increase in drag with large flap deflections as well as the difference in drag between positive and negative flap angles of the same magnitude. Positive deflections produced significantly more drag for a given angle of attack which was expected for an airfoil with positive camber. Figure 5 also shows the data for pitching moment which were consistent with expected trends. The only noticeable trait was the decreased slope for large negative deflections, especially for the -30 deg. case, which also shows non-linear behavior with almost constant C_m near and after stall.

B. Tabbed Cases

Following the fixed-tab cases, the tab was actuated for each of the flap deflections and surface pressure, lift, drag, hinge moment and pitching moment data were taken. The consequences of using a tab to hold or move a flap could then be determined. In this section data will be shown for select cases of 0 and ±10 degrees flap deflection. The 0 deg. case will demonstrate the general effect of a tab on the NACA 3415 airfoil while the ±10 deg. cases will further show these effects as well as the capabilities of the tab in assistance of the flap under a non-zero flap setting. The larger tab deflections of ±45 and ±60 deg. are not presented as a part of these studies as they were not effective due to complete flow separation on the tab for the entire range of angle of attack.

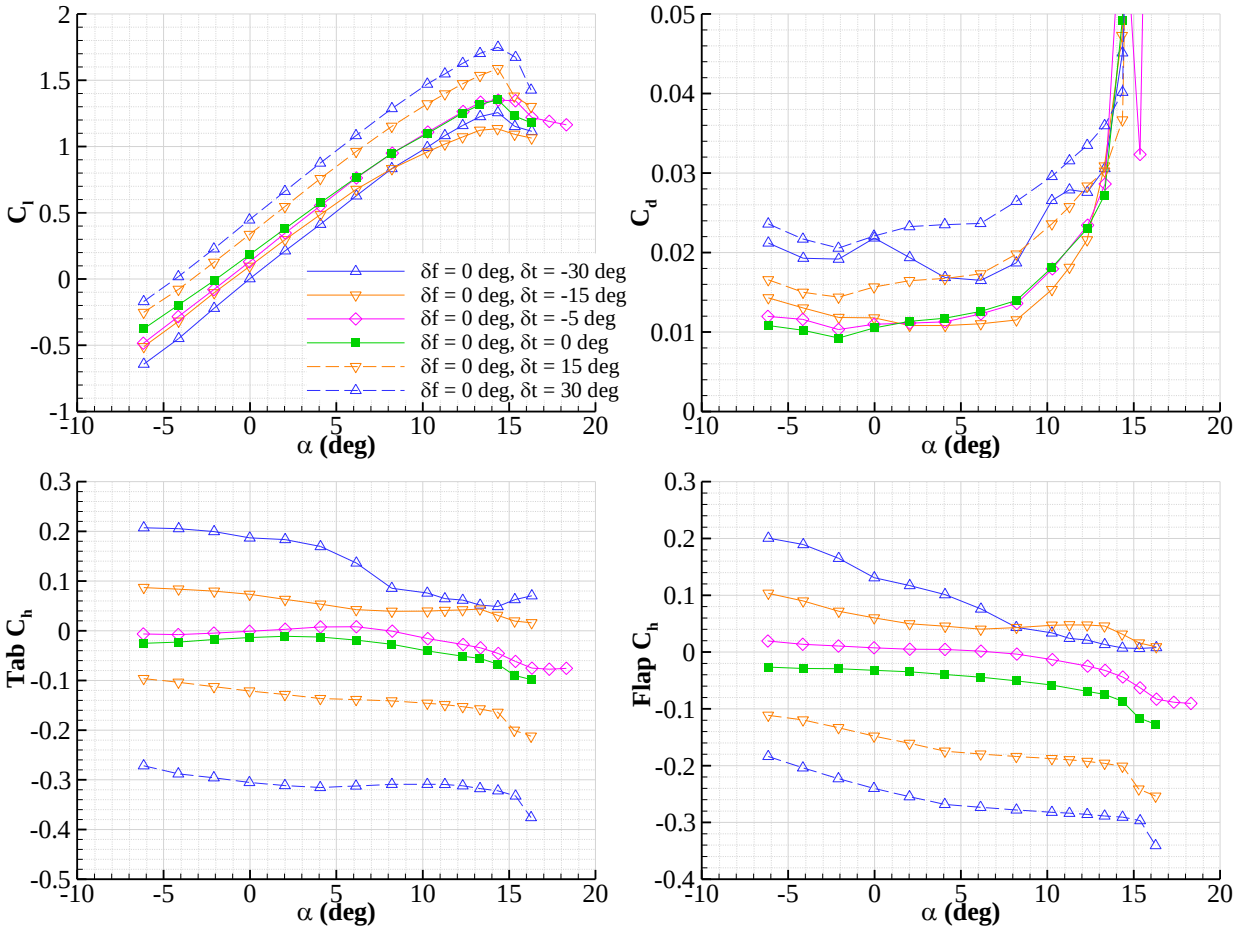

Figure 6. NACA 3415 performance with 0 deg. flap deflection and range of tab deflections.

From the data presented above in Fig. 6, it can be seen that a 25%-flap simple tab has a large effect on the performance of the NACA 3415 airfoil. A 30 deg. tab deflection increased $C_{l,max}$ by 29% while only a -15 deg. tab deflection reduced it by 16%. The drag data also indicate a large effect with both the positive and negative 30 deg. deflections doubling the drag over the linear range of angle of attack. There is a slight decrease in drag for higher angles of attack for the -30 deg. case.

This case also displayed different trends for the hinge moment data of both control surfaces compared to the other tab deflections. This occurs during the same range of angle of attack as the decrease in drag. Over this range, the slope of the hinge moment curve is more negative than the previous -15 deg. deflection and actually becomes positive post-stall. The other cases exhibit a drop in hinge moment post-stall. As for hinge moment coefficient magnitudes, both the positive and negative 30 deg. tab deflection produce a ΔC_h of 0.2 in the flap hinge moment coefficient for the lower range of angles of attack (α = -5 to 5 deg.). This effect is reduced for larger angles of attack for the δt = -30 deg. case but is maintained for the 30 deg. case. The tab hinge moment coefficients resemble the flap data with the exception of the 30 deg. tab deflection, which has a larger negative hinge moment.

With the data presented for zero degree flap deflection to show the general influence of the tab on the NACA 3415 performance, data will now be presented for ±10 deg. flap deflections to demonstrate the tab effect

under non-zero flap deflections. An additional tab deflection of 5 deg. was included to provide another tab deflection that produces a flap hinge moment around zero.

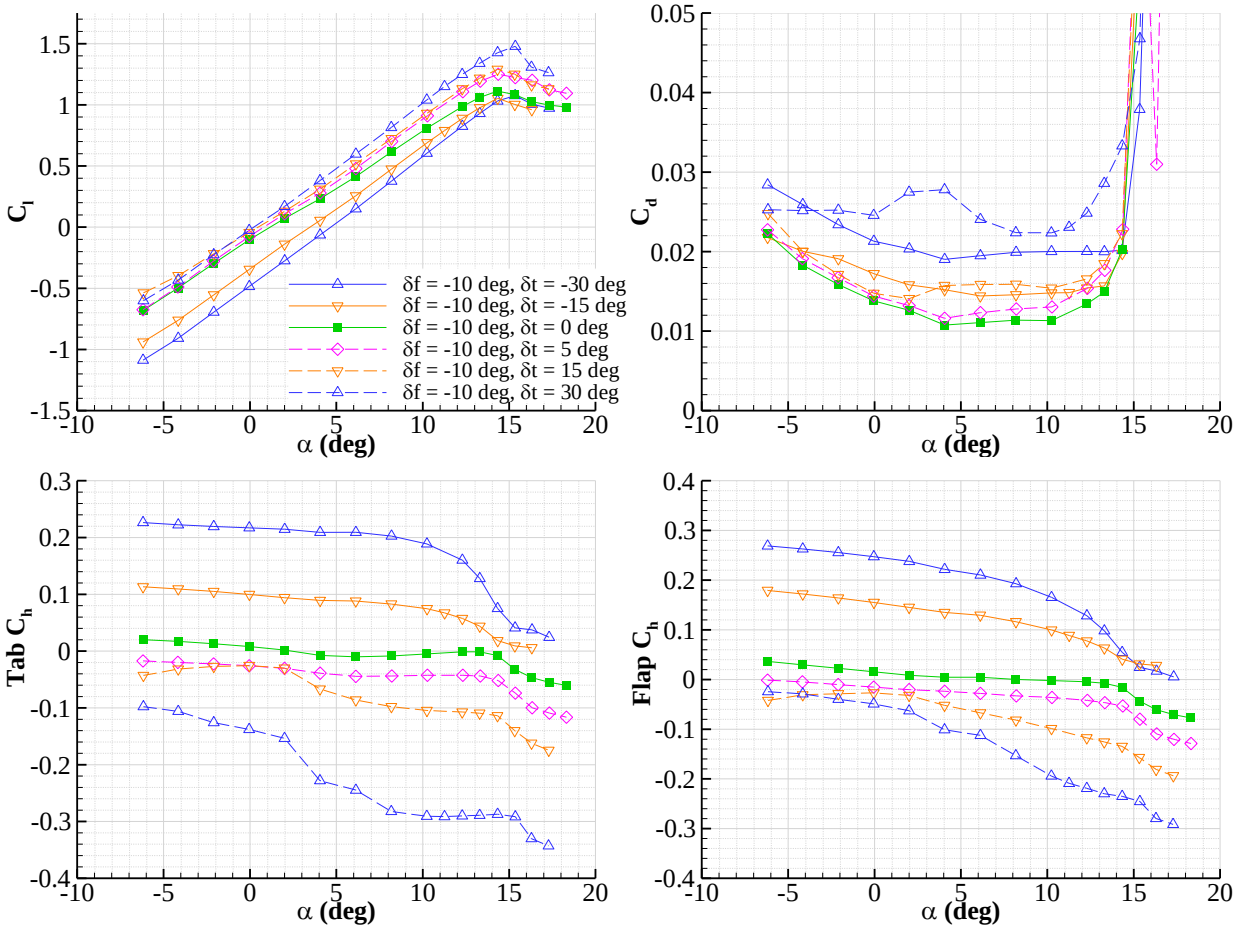

Figure 7. NACA 3415 performance with -10 deg. flap deflection and range of tab deflections.

As shown above in the data for a -10 deg. flap deflection, the tab continues to have a significant effect on the airfoil performance but several differences can be seen compared to the 0 deg. flap deflection case. Starting with the lift data, there is even less symmetry about the fixed tab data. Even though this is expected since the airfoil has positive camber, the lift curve slope behavior changes when the tab is deflected in either direction. Additionally, each of the negative tab deflections, while offsetting the lift curve as expected, do not influence the magnitude of $C_{l,max}$.

Changes in behavior can also be seen in the hinge moment data for both the tab and the flap, especially for the tab hinge moment coefficient data. For δt = -30, -15, 0 and 5 deg., the slope and post-stall behavior are similar while the tab deflections of 15 and 30 deg. exhibit a drastic change in slope at around 2 deg. angle of attack then flatten out at 10 deg. angle of attack. From flow visualization results, this was due to the influence of the separation that occurs on the lower surface of the flap for low angles of attack. This separation then reattaches on the tab with increasing angle of attack which induces an abrupt decrease in hinge moment.

The flap hinge moment data show the same behavior for the same two positive tab deflections but is not as pronounced as in the tab data. The tab is less effective for lower angles of attack when positively deflected, while the negative deflections are the most effective in this range. This result is reversed for the larger angles of attack near stall as well as post stall. It is also interesting to note that little tab deflection is required to hold the flap at -10 deg. since the flap hinge moment remains near zero for the entire range of angle of attack before stall. Furthermore, the hinge moment required to hold this deflection is also near zero since the tab hinge moment is almost zero. A 5

deg. tab deflection was tested to produce this effect but actually induces a slight negative flap hinge moment for all angles of attack.

Lastly, the drag data results were as expected with the larger deflections having the same order of effect as seen for 0 deg. flap deflection. A bump in the drag for the 30 deg. tab deflection for larger angles of attack was seen while the other tab deflections show a similar pattern.

To demonstrate the effect of a tab for a positive flap deflection, data are shown below in Fig. 8 for 10 deg. For this flap deflection, an additional tab deflection of -10 deg. was run to provide additional data in the region of flap $C_h = 0$.

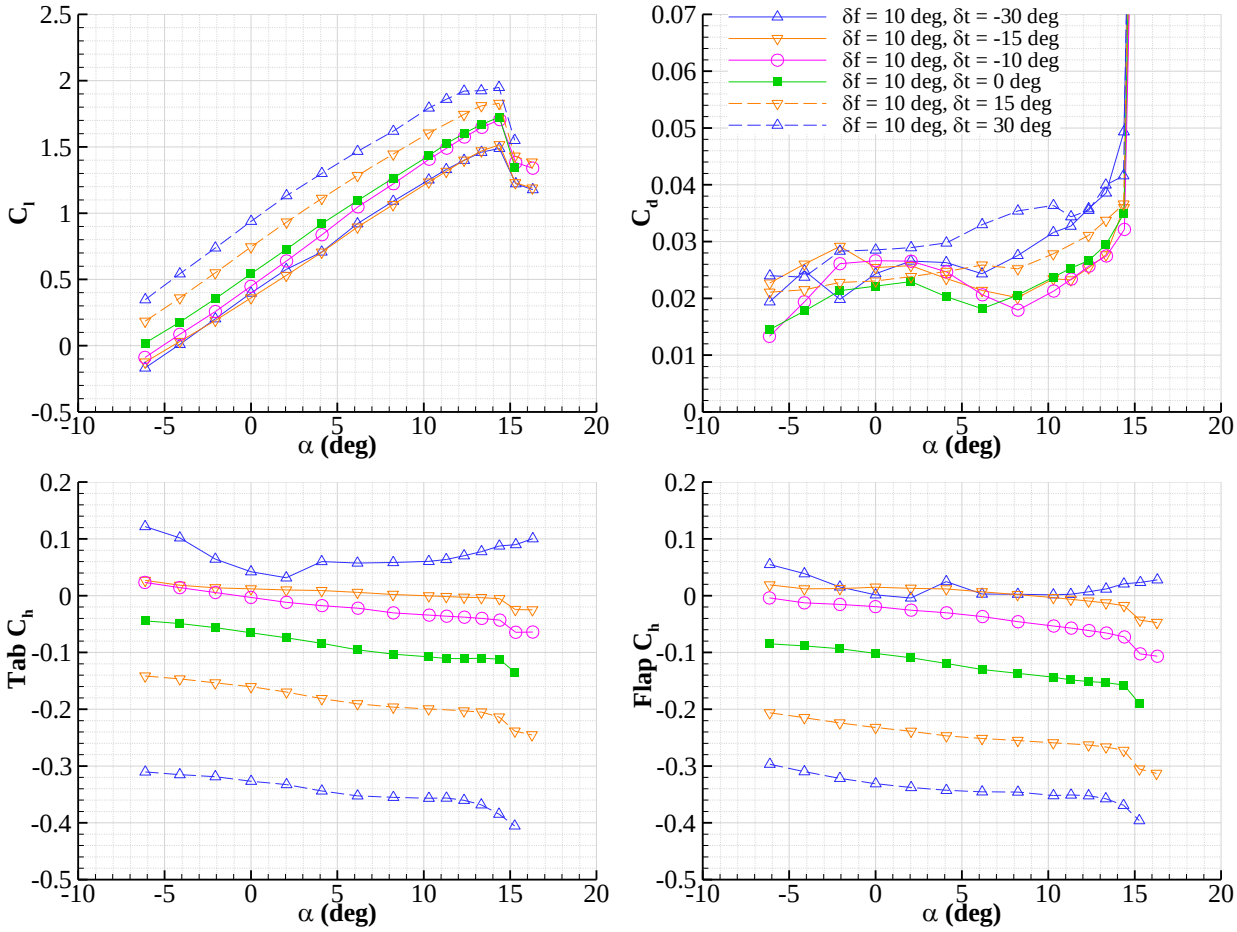

Figure 8. NACA 3415 performance with 10 deg. flap deflection and range of tab deflections.

Beginning with the lift data, negative tab deflections larger than -15 deg. produce no change in $C_{l,max}$ or in the general lift behavior. In contrast, a 30 deg. tab deflection increases $C_{l,max}$ by 13%. The stall angle of attack remains constant for all tab deflections tested. The drag data, while non-linear, shows the same trend for each negative tab deflection. This trend of decreasing drag with increasing angle of attack begins at roughly the same α for each of the deflections with the magnitude of reduction varying. The positive deflections follow the same trend before the observed decrease in the negative deflections but continue to increase before stall.

As was seen with the -10 deg. flap deflection case, the hinge moment data for the 10 deg. deflection reveals a sharp change in behavior between different tab deflections. Here the -30 deg. tab deflection displays non-linear performance with increasing angle of attack as well as a positive increase in hinge moment post-stall which was not seen for the other tab deflections. This same behavior was seen on both the flap and the tab while the other tab deflections all show expected data. Again, the separated flowfield seen on flap and tab deflections of the opposite sign is the cause of the non-linear behavior.

Analyzing the flap hinge moment data, the -15 deg. tab deflection is the most effective at producing a zero flap hinge moment for most angles of attack. Interpolating between the curves for -15 deg. and -10 deg., assuming

linear behavior between curves, the exact deflection for holding the flap deflection could be found. The penalty in tab hinge moment for flap assistance is actually small since a small positive hinge moment is seen for lower angles of attack until around α = 6 deg. then is near zero until stall. Further analysis will be provided later in the results and discussion section and will also account for lift and drag.

C. Computational Results

The CFD results will be compared to the experimental data using the tripped boundary layer data when available. The primary metrics of concern are the lift and drag coefficients, as well as the flap hinge moment. The flap hinge moment will be related to the power required to actuate the control surface, and this will be used as an initial screening of the powered tab concept.

In Fig. 9, the lift, drag, and hinge moments are compared to the tripped experimental data, respectively, for the δf = 0, ±10, and ±30 deg. and δt = 0 deg. configuration. For δf = 0 deg. and δt = 0 deg. there is excellent agreement up until stall (~14 deg.), where the CFD is seen to break much more gradually than the experiment. This is typical for steady-state CFD at high angle of attack. In particular, the lift is seen to be over-predicted after stall and the drag under-predicted. However, CFD is capturing both the magnitude and trends of the forces and moments as the angle of attack is varied, giving confidence in the ability of CFD to predict increments when the powered tab is simulated later in this work.

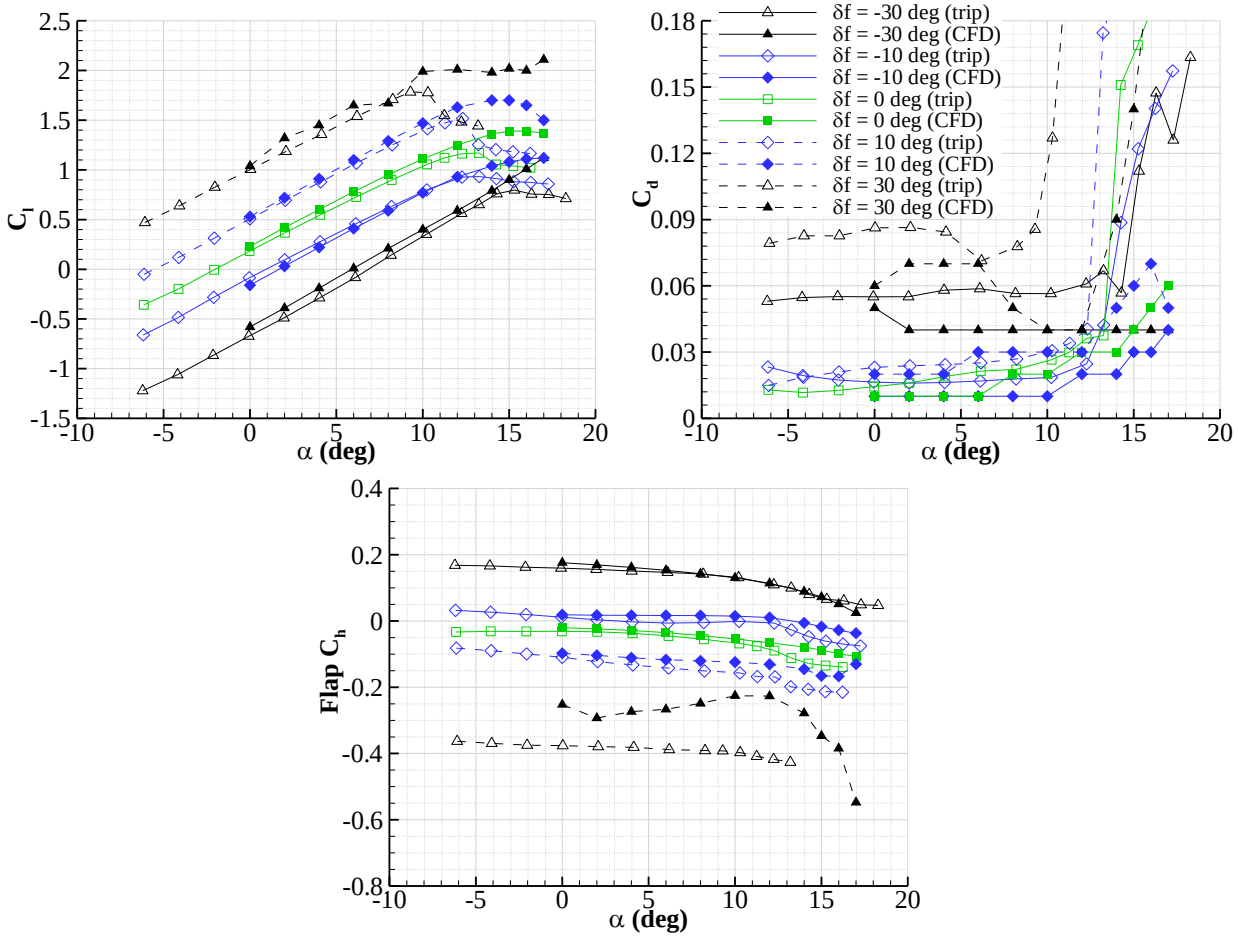

Figure 9. CFD vs. experimental tripped data comparison for select flap deflections and δt = 0 deg.

The same comments can be made at higher flap deflections, such as the δf = 10 and δt = 0 deg. configuration shown in Fig. 9. Agreement between CFD and experiment is seen to be excellent up until 13 deg. It can be argued that the steady-state assumption is no longer valid at high angle of attack when the flow is massively separated behind the airfoil. Regardless, the trends are predicted and there is generally good agreement between the CFD and experiment.

At δf = 30 deg. and δt = 0 deg., the flow is becoming highly unsteady as can be seen in the CFD data. There is large scale separation in these greater flap deflections which is not properly modeled in a steady-state simulation, and not surprisingly, the comparison between CFD and test tends to wander as the flap deflection is pushed to greater levels.

Negative flap deflections are also of interest, and were simulated in both CFD and experiment. The comparison for δf = -10 and δt = 0 deg. is also shown in Fig. 9. Excellent overall agreement is seen. As in the positive flap deflections, we see the CFD break more gently at stall than experiment. As the negative flap deflection increases to -30 deg. with δt = 0 deg. we see the CFD data begin to deviate from the test data. In fact, the CFD is not showing any break in the lift at high angle of attack for this configuration, whereas the test indicates a stall around 15 deg.

Tab deflections are of primary importance to this study. Up to this point, we have only compared zero tab deflections to experimental data, and have seen good agreement between CFD and test except where the flow is known to be separated. Note the experimental data are not tripped in these configurations. Therefore, it is expected that there will be laminar to turbulent transition effects which will not be captured in the fully-turbulent CFD. The flap and tab combinations examined were (δf = -10 deg., δt = 30 deg.), (δf = 0 deg., δt = -5 deg.), and (δf = 10 deg., δt = -30 deg.) and are shown below in Fig. 10. The δf = -30 deg. and δt = -30 deg. case will also be shown later.

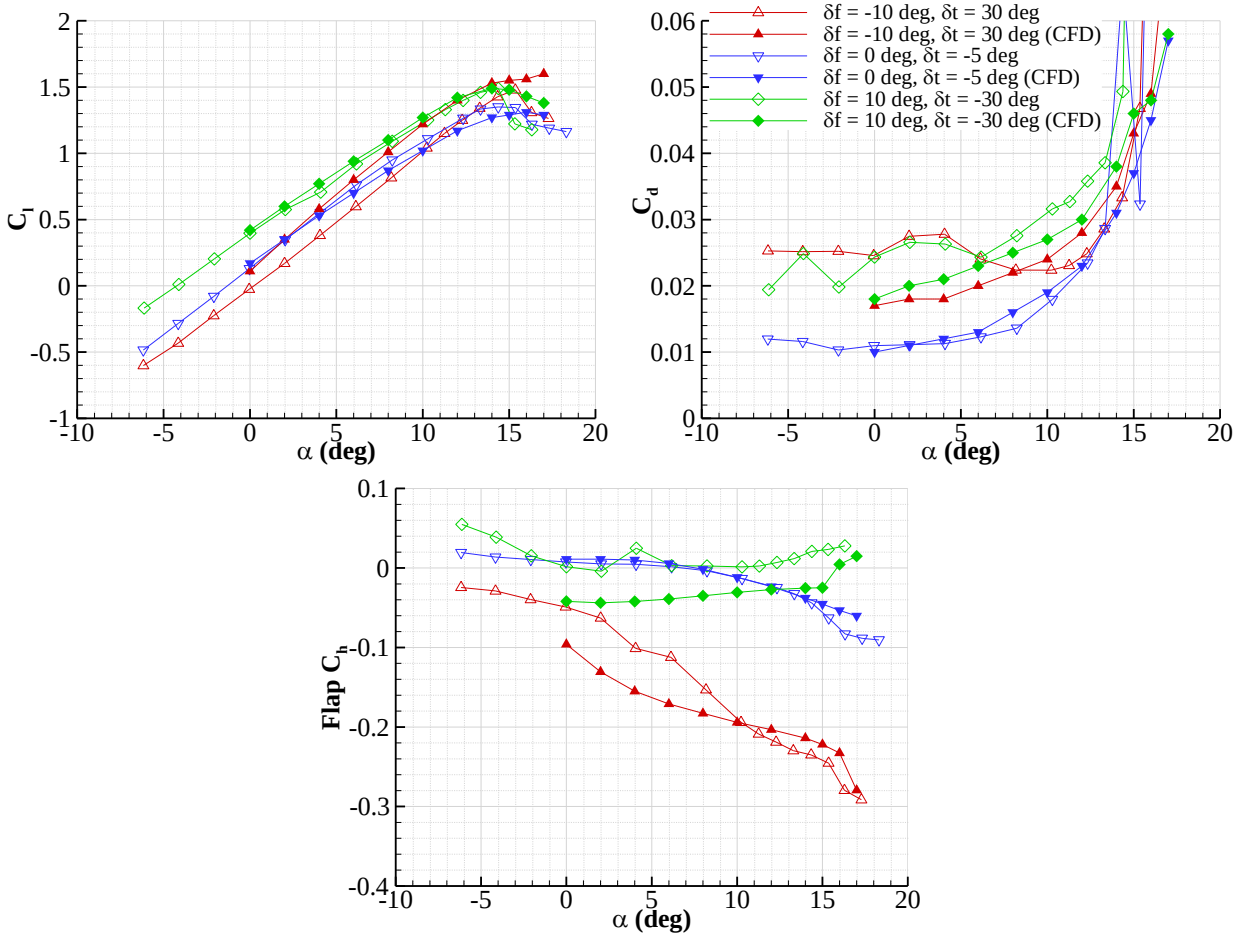

Figure 10. CFD vs. experimental data comparison for select flap and tab deflections.

In Fig. 10, the CFD and test data are compared for the δf = 0 and δt = -5 deg. case. Excellent agreement is seen, as has been typical for small deflections. The CFD is seen to break more gently at stall than experimental data, but the stall seems to occur at the same angle of attack in both CFD and test. Continued good agreement is seen for the more challenging configuration of δf = 10 and δt = -30 deg. The same statements can be made about this configuration as the prior configuration. The δf = -10 and δt = 30 deg. configuration was examined next. The

agreement is good, with the CFD slightly over-predicting the lift. However, note the inflection point in the hinge moment near α = 15 deg. is correctly captured in the CFD.

The next case considered is probably the most challenging with the δf = -30 and δt = -30 deg. configuration. The lift, drag, and hinge moments can be seen below in Fig. 11. The steady-state CFD is seen to over-predict the lift as well as miss the "drag bucket" phenomena seen in the experimental data between 5 and 15 deg. angle of attack. The hinge moment is seen to have the correct trends, but a lesser moment is seen in the CFD than test. At this condition, the CFD does not capture the stall seen in the experiment. With the understanding that some of these differences can probably be attributed to transition, as seen with flow visualization, the other differences are due to the unsteady nature of the flow.

Knowing that the steady-state CFD would likely not compare well on configurations which have large flap/tab deflections and therefore, separated flow, unsteady CFD was planned as part of this work for select cases. The authors chose to run DDES with a low dissipation scheme on the δf = -30 deg., δt = -30 deg. case at α = 0 and 10 deg.

The unsteady results for lift are also shown in Fig. 11 for lift and drag. Note the improvement when the simulation is run in a time-accurate fashion. The lift predicted by the unsteady CFD closely matches the test data. It is therefore reasonable to assume many of the other configurations where the CFD was slightly high in lift could have been improved by running time-accurate.

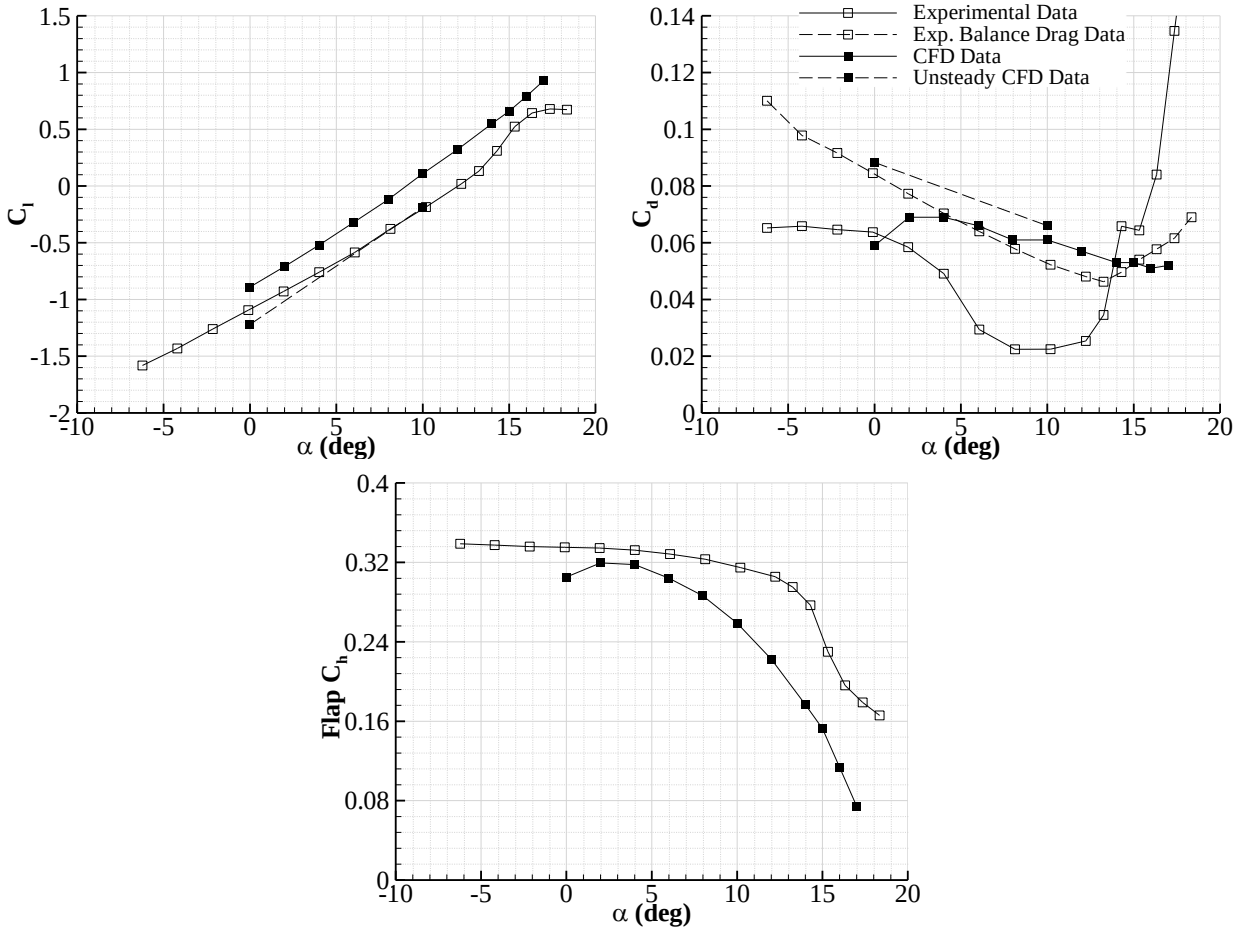

Figure 11. CFD vs. experimental data comparison for δf = -30 deg. and δt = -30 deg. with additional unsteady CFD data.

The drag behavior on this configuration is most interesting. A drag bucket is seen between α = 5 and 15 deg. The steady-state CFD did not predict this trend. However, the unsteady CFD did show a decrease in drag from 0 to 10 deg. angle of attack. Without more unsteady CFD data, it is not possible to discern a "bucket" profile. However, the unsteady CFD did compare better with the drag balance data. However, previous unflapped airfoil

experiments have shown the balance data to be consistently higher than the wake data due to 3-D effects associated with the small gaps between the model and test section ceiling and floor. Flow visualization was required to fully understand this phenomenon, and the results show that it appears to be due to laminarization of the lower surface, which the CFD completely ignores due to the fully-turbulent assumption.

It is customary to show a flow visualization picture of the CFD solutions for DES/LES predictions, if only to give the reader a notion of the length scales seen in the flow. A more trained eye will also examine the flow visualization (typically cuts of vorticity or other gradient-based vortex detection metric) for evidence of numerical wiggles and sudden jumps in grid density. Such visualizations are shown in Figs. 12 and 13 for α = 0 and 10 deg., respectively. The Q-criteria is used to identify the turbulent structures, which are then shaded by Mach number for clarity. At α = 0 deg., the structures in the wake are organized into von Karman streets, typical for shedding at low angle of attack. At higher angle of attack, we see this organization break down and the flow behind the airfoil to be highly separated and rich with eddies of various length scales.

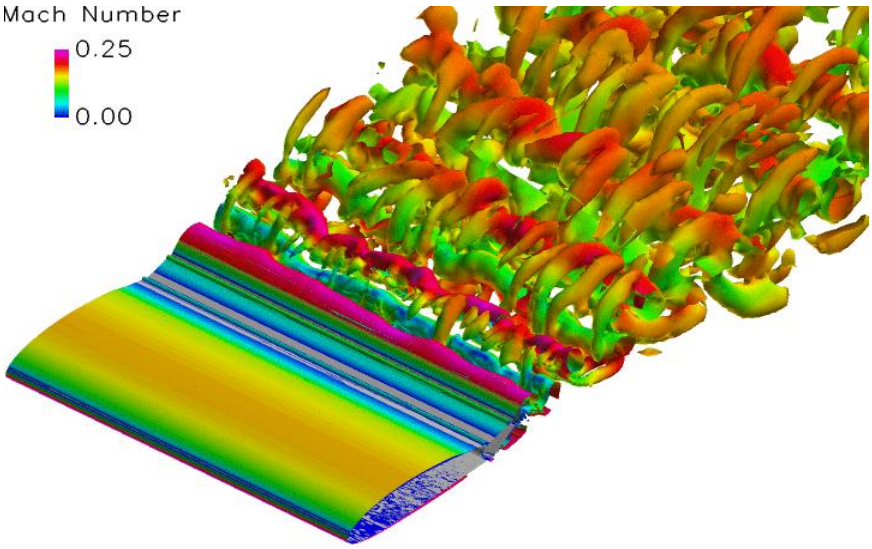

Figure 12. Q-criteria for δf = -30 deg. and δt = -30 deg. case at α = 0 deg.

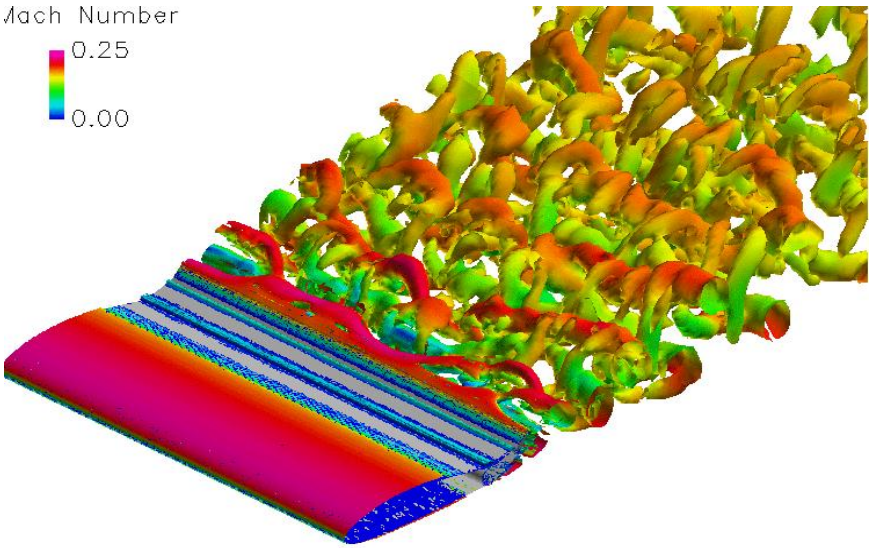

Figure 13. Q-criteria for δf = -30 deg. and δt = -30 deg. case at α = 10 deg.

D. Discussion on Power-saving Results

The data from the tabbed cases were compared to the data from the baseline case to assess the power savings of a tab-assisted flap. To begin, since the tests were solely static in nature, measuring data for a fixed tab and flap deflection for an angle of attack range, only changes in lift, drag and hinge moment could be calculated directly. Later, a dynamic analysis looking at the work savings for a simulated flap and tab deflection scenario will be presented. For the hinge moment calculations, the hinge moment coefficient was used along with geometry to calculate the dimensional hinge moment in order to make a direct comparison between the flap and tab. To calculate the tab deflection for trim, linear interpolation was used between tab deflection curves, which was deemed reasonable for tab deflections between ±30 degrees. The results of these calculations for flap deflections of -10 and 10 deg. and respective tab deflection for "trim" are presented below in Table 2. The calculated reductions/increases in hinge moment, lift and drag are relative to the "untrimmed" case.

Table 2. Effect of using tab on flap hinge moment

δf (deg.)	*α (deg.)*	δt_{trim} *(deg.)*	*% Reduction in Hinge Moment*	*% Drag Change*	*% Lift Change*
-10	-4	4.24	97.15	3.31	1.66
	-2	3.40	96.61	3.8	5.56
	0	2.49	96.14	2.17	13.76
	2	1.49	94.17	1.59	15.57
	4	0.84	81.4	1.85	3.96
	6	0.73	76.77	1.8	3.23
10	-4	-12.33	97.88	-3.33	-62.82
	-2	-12.73	98.48	9.81	-39.44
	0	-12.93	99.06	13.06	-29.50
	2	-13.44	99.42	7.86	-25.35
	4	-13.74	99.61	11.76	-22.39
	6	-14.23	99.74	15.3	-18.17

The results for the ± 10 deg. cases show the significant effect the tab has in reducing the hinge moment for holding a flap deflection. For all but two cases above, the hinge moment reduction is above 95% of the untrimmed value even though the tab deflections are ranging from -10 to -15 degrees for the 10 deg. flap deflection. The tab deflections required for trim for the -10 deg. flap deflection are quite low ranging from 1 to 4 deg. but holding these smaller tab deflections requires a larger hinge moment than that for the 10 deg. flap deflection. From the data shown in Fig. 6 above, it was seen that the tab deflection for trim reduced the hinge moment coefficient from -0.1 to zero and required very little hinge moment to hold this tab deflection. Thus, the hinge moment reduction was almost 100% for 10 deg. flap deflection. For the -10 deg. flap deflection, the same was true for the tab hinge moment but the flap hinge moment was already near zero and therefore required only a few degrees with the tab. This resulted in slightly lower hinge moment reductions.

The consequence of these very high hinge moment reductions is the increase in drag and loss/increase in lift. Starting with the -10 deg. flap deflection, only a few degrees of tab deflection increase lift up to 16%, which is a loss of effectiveness for a negative deflection. As expected, the drag is only slightly increased by the tab deflection. The effects are magnified for the 10 deg. flap deflection since it requires larger tab deflections for trim. For the angles of attack above zero, the lift is reduced from 18 to 30%. The reasoning for the larger reductions for angles of attack below zero is the fact that the lift is near zero resulting in a high relative change in lift. The drag increase is larger in this case as well even though one case (α = -4 deg.) resulted in decreased drag.

While only a small sampling of data was presented in Table 2, the trends seen for the other flap deflections remain the same. For the positive flap deflections, the hinge moment reductions remain above 99% for each tab deflection. The complex flowfield existing for coupled positive/negative flap and tab deflections is most likely the cause of this large reduction. For flap deflections above 10 deg., separation is seen and, with increasing flap

deflection, occurs for a larger angle of attack range. The same is observed with higher tab deflections and, when combined with large flap deflections, yields a completely separated flowfield over the tab. This flowfield induces a minimal hinge moment on the tab while effecting a large change in the flap hinge moment.

While this is effective for power savings, the consequences are again seen in the lift and drag. With increasing flap deflection and increasing required tab deflections, the drag increases greatly approaching 40% for the 30 deg. flap deflection case. In addition, the lift loss is consistently above 30% approaching 40%, ignoring angles of attack where C_l is small, for 30 deg. flap deflection. While the hinge moment reductions are slightly lower for the negative deflections, the lift and drag penalties are almost equivalent to that of the positive deflections. Since the change in the lift is substantial, a study was done using flow visualization as well as the C_p distributions to examine the cause. This study is discussed later in this section.

Next, a simulated dynamic study was done since the static data and hinge moment reductions do not sufficiently represent the eventual application. As stated earlier, since dynamic movements of the tab and flap system were not implemented in this phase of testing, accurate dynamic hinge moments as well as a time schedule for the deflections are not available for power savings calculations. As an estimate of potential work savings, several hypothetical cases of flap deflection schedules could be analyzed using the static data and assuming linear behavior between flap and tab deflections. Again, this is a reasonable assumption for all but the larger ±45 and ±60 degree deflections.

The selected hypothetical cases were deflecting the flap from 0 deg. to 30 deg. and back to 0 deg. The opposite case in going to -30 deg. and back was also included. Three angles of attack (α = 0, 4 and 8 deg.) were analyzed and the tab was limited to ±30 deg. deflections. Once the desired deflection was reached, the tab would straighten out and additional work required to hold deflection was ignored.

The baseline calculation was made with the flap hinge moment coefficient data for each of the deflections tested. From an integration of flap C_h vs. flap deflection for each angle of attack over the range of the desired deflection, a value could be obtained which, along with geometry and flow conditions, leads to the work done to complete the deflection. The data used for these calculations are shown below in Fig. 14. Flap hinge moments that aided flap movement were ignored and work was assumed to be zero for that segment.

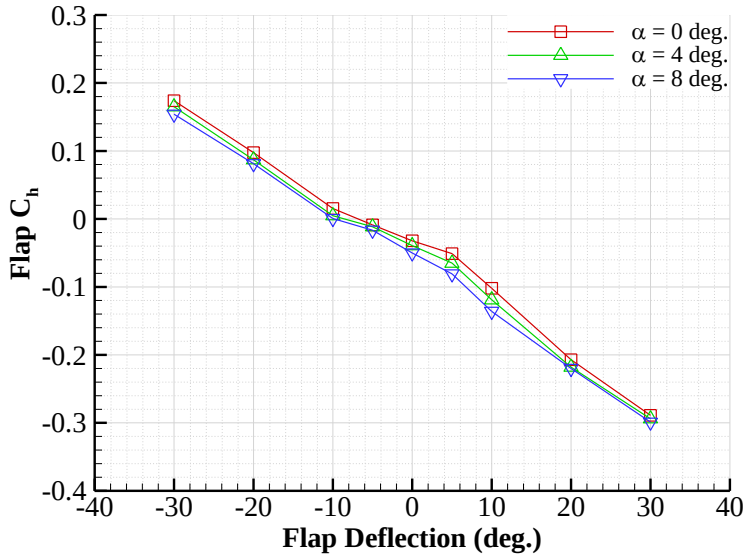

Figure 14. Flap C_h vs. flap deflection for α = 0, 4 and 8 deg.

For the tabbed case, since only 0 and ±30 tab deflections were allowed, a tab schedule was first determined for each desired flap movement. For example, a desired flap movement from 0 to 30 deg. would require a -30 deg. tab deflection until reaching 30 deg. in which the tab would be retracted to 0 deg. In order to find the work required for this movement, an integration of tab C_h vs. flap deflection under a tab deflection of -30 deg. would be calculated and, as before with the flap calculations, would be converted to work with the flow conditions and tab geometry. To effect movement of the flap back to 0 deg. a tab deflection of 30 deg. would then be required and the same process would be used to calculate work. Additionally, the work required to deflect the tab from 0 to -30 deg. at δf = 0 deg. and then from -30 to 0 deg. at δf = 30 deg. as well as the required movements for returning the flap to 0 deg. is

added. Again, assisting hinge moments would be ignored. The data used for the calculation of work for constant tab deflection vs. flap deflection is presented below in Fig. 15.

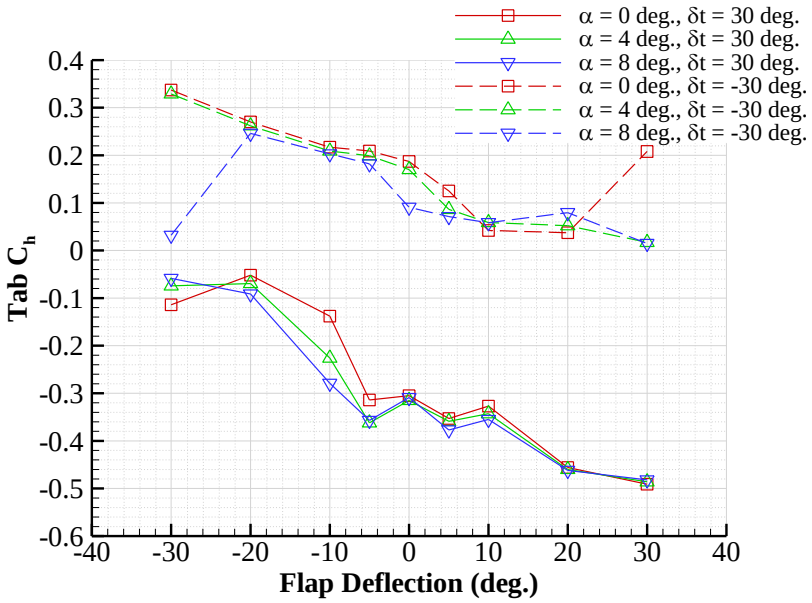

Figure 15. Tab C_h vs. flap deflection for α = 0, 4 and 8 deg. and δt = ±30 deg.

For both deflection scenarios, it was found that no work was required to return the flap to its original position at 0 deg. since the hinge moments were assisting. So the work savings calculations for obtaining the desired deflection represent the work savings for the entire scenario. The results of these calculations for the three angles of attack are listed below in Table 3, where the scenarios are denoted by the desired deflection in the table.

Table 3. Work savings for tab-assisted flap in percent

	α (deg.)		
δf (deg.)	0	4	8
0 to 30	92.9	93.7	95.0
0 to -30	80.7	80.5	78.6

The resulting work savings shown in Table 3 above are quite large but were expected due to the large hinge moment reductions observed in the static investigation. The drag effects were ignored for this study as well as the work required to hold the desired deflection with a tab deflection. In order to maintain the desired lift coefficient, which would be greatly affected by tab movement, either the angle of attack of the aircraft or flap angle would need to be adjusted. In any case, this simplified dynamic analysis proves the merit of using tab deflections to actuate the flap.

E. Loss of Flap Effectiveness Study

Previous data shown revealed a trend of large tab influence on the flap effectiveness necessitating additional analysis. This influence was seen as large changes in lift when using the tab for "trim" and, in some cases, reversal of effectiveness apparent in both lift and hinge moment data. To look at the latter effect, data from the ±30 deg. flap deflection cases were examined further since this effect is intensified with increasing flap deflection. For the 30 deg. flap deflection case, flow visualization was performed on two different tab deflections to diagnose the cause the reversal in flap effectiveness and large loss of lift. Then looking solely at the influence on lift, the lift change was tabulated for each flap deflection and corresponding tab for "trim." The C_p distributions for the 10 deg. flap deflection are also shown in support.

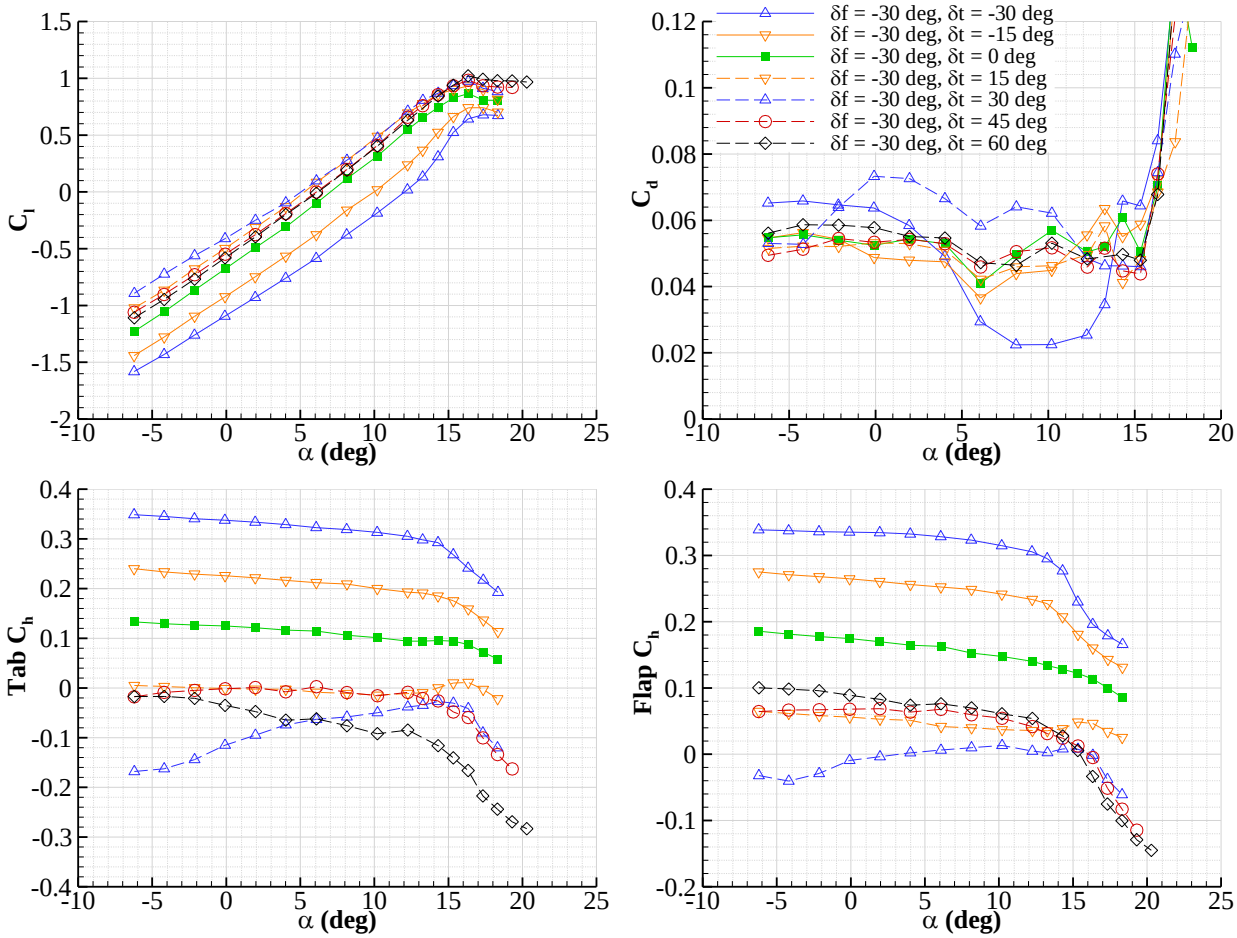

Figure 16. NACA 3415 performance with -30 deg. flap deflection and range of tab deflections.

Figure 16 above contains the aerodynamic performance results to the -30 deg. flap deflection case. The change in lift for decreasing (more negative) tab angle decreases almost to the point where additional tab deflection produces no additional effect. This was more evident for increasing (more positive) tab angle where by a tab deflection of 45 deg. there was a reversal of effectiveness and actually begins to produce less lift than a tab deflection of 30 deg. Increasing to a deflection of 60 deg. continues the effect with additional lift loss even though $C_{l,max}$ increases. This loss of flap effectiveness was also evident in both the flap and tab hinge moments for both the larger tab deflections which implied the separation on the tab decreases the hinge moment on the tab and erases its effectiveness on the flap.

The 30 deg. flap deflection case displays a more apparent reversal of flap effectiveness. Figure 17 shows the lift and drag coefficient data along with the flap and tab hinge moment coefficients.

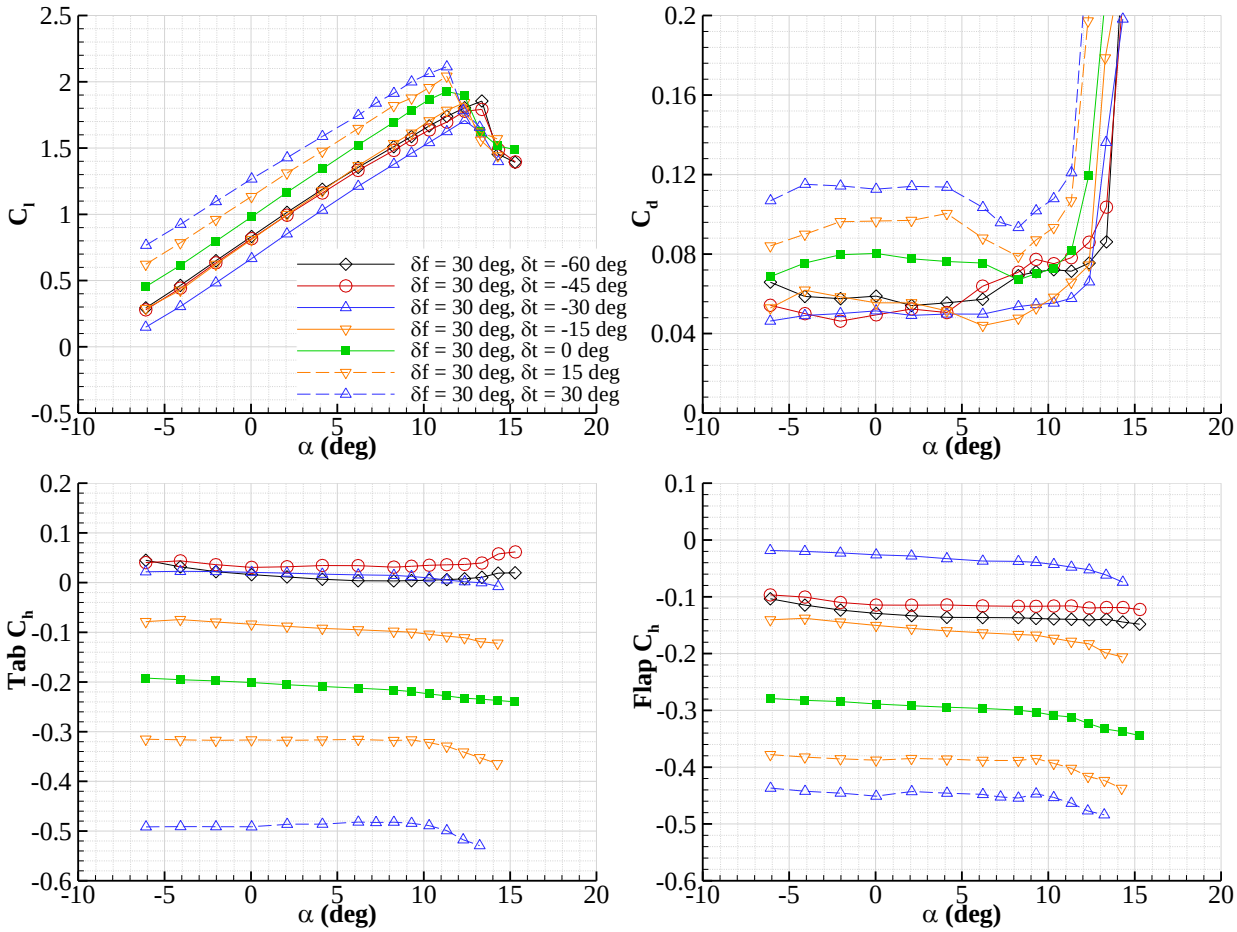

Figure 17. NACA 3415 performance with 30 deg. flap deflection and range of tab deflections.

The lift data seen in Fig. 17 shows evidence of this reversal where there is no additional effect due to the flap and tab past a tab deflection of -30 deg. The lift curves for δt = -45 and -60 deg. are almost equivalent to that of the -15 deg. tab deflection.

The data for flap hinge moment was as expected showing the same result as in the lift plot. The hinge moment data for the -45 and -60 deg. tab deflections almost replicate that of the -15 deg. tab deflection but have different behavior post-stall. That outcome in the tab hinge moment data is not as pronounced but occurs again past the same tab deflection of -30 deg. A slight reversal in flap effectiveness is not seen until δt = -60 deg.

Looking again at the tab effect on flap hinge moment, a zero flap hinge moment was accomplished by a tab deflection of approximately -30 deg. As shown, tab deflections of 45 and 60 deg. produce an adverse effect, thus making these deflections ineffective. The penalty in using this tab deflection for flap trim was seen in the lift reduction which was on the order of 30%.

To explain the adverse effect from the tab transitioning from δt = -30 deg. to the larger negative tab deflections, flow visualization was implemented. This technique provided insight into the flowfield around the airfoil and was performed at zero angle of attack for the tab at -30 and -45 deg. The results are shown below in Figs. 18 and 19.

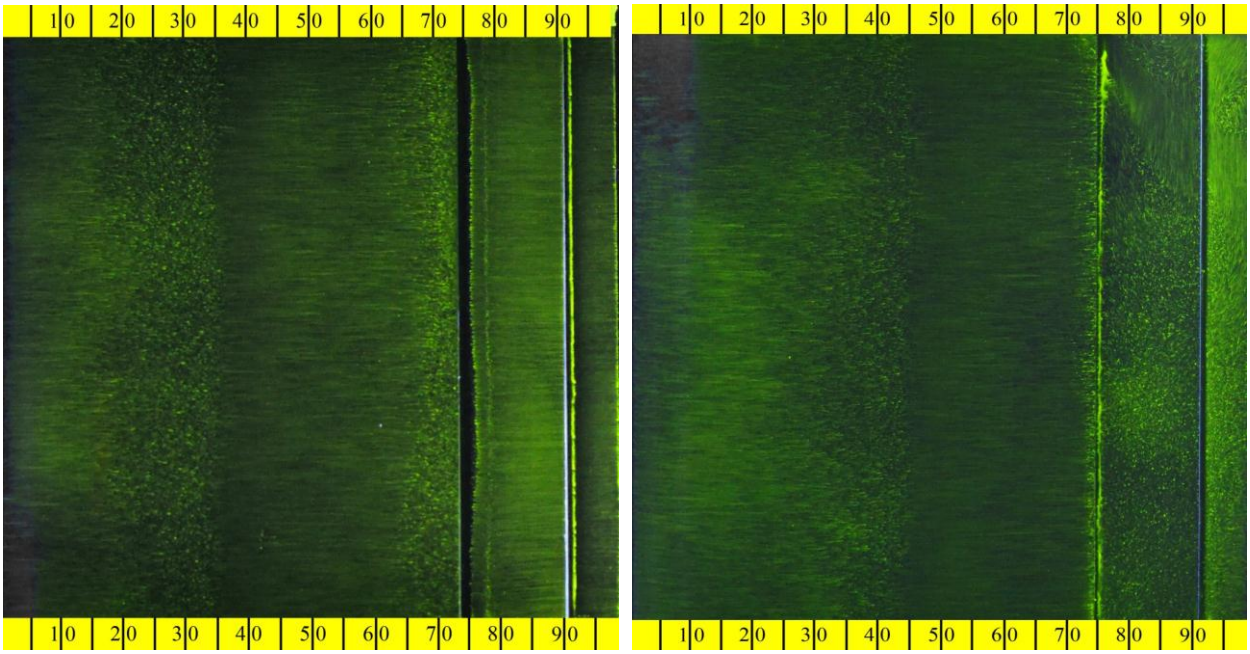

a) **b)**

Figure 18. Surface-oil visualization for 30 deg. flap and -30 deg. tab deflections on a) upper surface and b) lower surface.

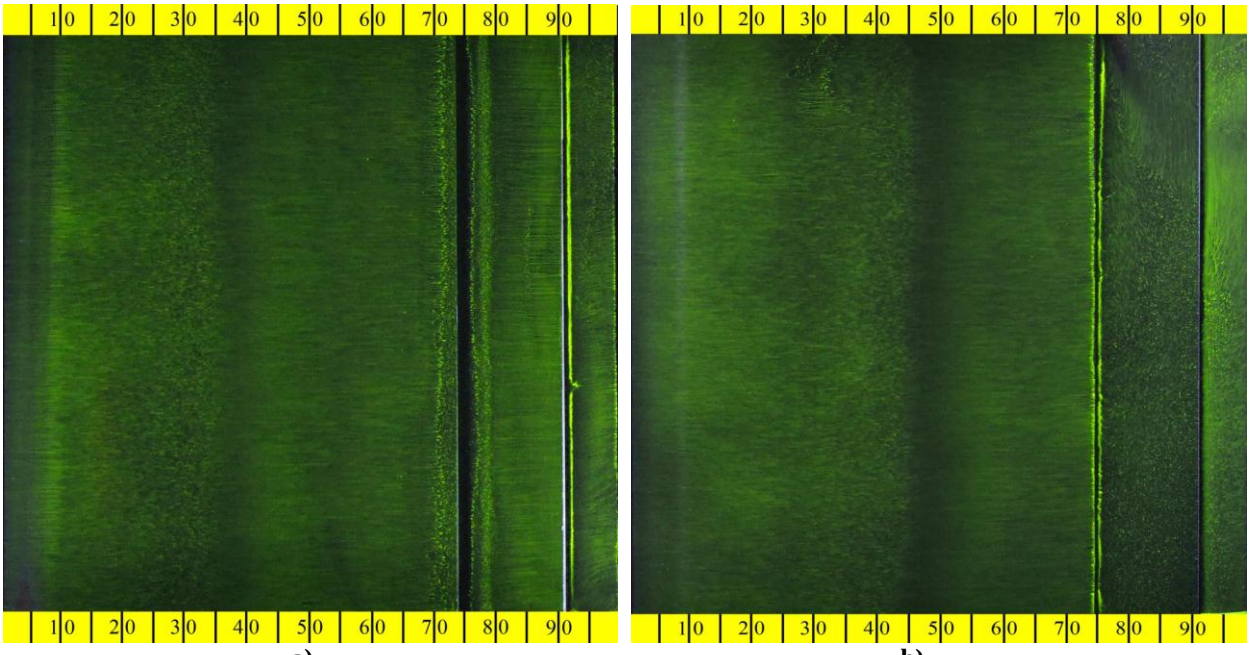

a) **b)**

Figure 19. Surface-oil visualization for 30 deg. flap and -45 deg. tab deflections on a) upper surface and b) lower surface.

These flow visualization images show that while the flow remains unchanged on the lower surface, separation begins to occur on the upper surface of the tab when deflected from -30 deg. to -45 deg. The separation is nonuniform on the surface with larger regions of attached flow, but is expected for such a large tab deflection. What is unexpected is the large effect this separation has on the lift and hinge moments for both surfaces, as seen

above in Fig. 17, as it cancels much of the effect of the tab deflection producing a lift curve and hinge moment equivalent to that of a 15 deg. tab deflection.

This loss of flap effectiveness, with respect to the lift, was not limited to the ±30 deg. flap deflections since each flap deflection exhibited this effect. For each flap deflection tested, the change in lift from the untrimmed to trimmed case was calculated at zero angle of attack. A tab deflection for trim for the 30 deg. flap deflection case did not exist due to the reversal of flap effectiveness and lack of tab deflections run between 30 and 45 deg. Therefore, the closest tab deflection for trim was -30 deg. which produced a flap C_h of -0.026. Table 4 below contains the results of this study.

Table 4. Loss of flap effectiveness with use of tab for trim.

δf (deg.)	δt_{trim} (deg.)	C_l		% Reduction in $\lvert C_l \rvert$
		untrimmed	*trimmed*	
-30	27.92	-0.671	-0.405	39.6
-20	16.71	-0.429	-0.254	40.8
-10	2.49	-0.100	-0.086	13.7
-5	-1.22	0.012	-.00020	102.0
0	-4.06	0.186	0.133	28.5
5	-7.71	0.346	0.320	7.5
10	-12.93	0.542	0.382	29.5
20	-24.23	0.810	0.550	32.1
30	-30	0.977	0.663	32.1

For each flap deflection except for 5 deg., the effect on lift was substantial (14% to 102%) even though the 102% change for the -5 deg. flap deflection is due to the small amount of lift generated for this case. The larger flap deflections see the largest effect since large tab deflections are required for trim. Even smaller flap deflections with smaller tab deflections required for trim displayed a significant effect, such as the δf = 10 and δf = 0 cases. For the 10 deg. flap deflection, the C_p distribution for both the trimmed and untrimmed cases is shown below in Fig. 20. With the C_p distribution, the tab effect on the rest of the airfoil can be understood.

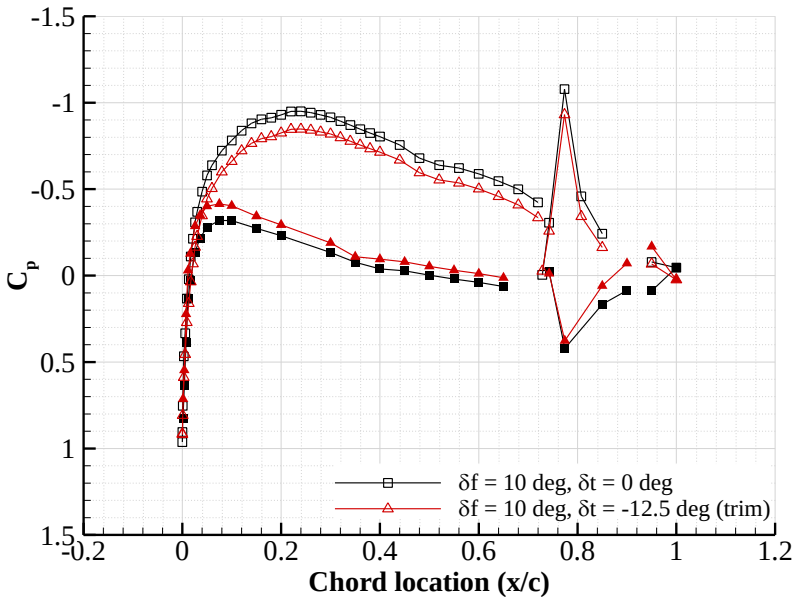

Figure 20. C_p distribution of 10 deg. flap deflection for baseline and tab trimmed cases.

The C_p distribution shows that, when the tab was deflected, the surface pressures reflect the roughly 15% reduction in lift over the entire main element. Though the tab is small, it's effect propagates forward across the

airfoil creating a significantly lower peak and a consistent offset in C_p across both the lower and upper surface. This is a significant effect for a tab deflection of only 12.5 deg.

V. Summary and Conclusion

This paper has presented a study on the feasibility of an airfoil model with a tab-assisted flap used to reduce control power. Two cases were studied: flap with a fixed tab (baseline) which represents the zero tab deflection case as well as the tabbed case, where the tab is actuated to induce zero hinge moment on the flap. From this study, the following conclusions were drawn:

- Using a tab for assisting the flap resulted in large hinge moment reductions but at the cost of higher drag and significant changes in lift.
- A study of flap deflection scenarios revealed potentially high reductions in work required.
- Overall, the tab had a large influence on the flap effectiveness resulting in large changes in lift. At the largest tab deflections, the influence resulted in a reversal of effectiveness in the lift and hinge moment.

To fully understand and quantify the benefits of a tab-assisted flap system, future experiments are to be undertaken on true real-time/dynamic flap and tab deflections for accurate simulation of control surface movement and calculations on power consumption. Initial work has been done in preparation for these tests and has shown the difficulty in accurately simulating full-scale deflection schedules at the proper reduced frequency.

Acknowledgments

This research was funded by The Boeing Company. The authors would like to thank Phillip Ansell at the University of Illinois for his assistance with the wind-tunnel operation and work designing the LabVIEW software. The authors would also like to thank Greg Milner and Dustin Burns in the University of Illinois Department of Aerospace Engineering Machine Shop for their work manufacturing the necessary components for the flap and tab as well as for the flap and tab actuation system.

References

[1] Holtzclaw, R.W. and Crane, R.M., "Wind-Tunnel Investigation of Ailerons on a Low-Drag Airfoil III – The Effect of Tabs," NACA ACR No. 4H15, 1944.

[2] Jones, R.T. and Nerken, A.I., "The Reduction of Aileron Operating Force by Differential Linkage," NACA TN-586, 1936.

[3] Soulé, H.A. and Hootman, J.A., "A Flight Investigation of the Reduction of Aileron Operating Force by Means of Fixed Tabs and Differential Linkage, with Notes of Linkage Design," NACA TN No. 653, 1938.

[4] Harris, T.A., "Reduction of Hinge Moments of Airplane Control Surfaces by Tabs," NACA Report No. 528, 1936.

[5] Ansell, P.J., Bragg, M.B., and Kerho, M.F., "Envelope Protection System Using Flap Hinge Moment Measurements," *28th AIAA Applied Aerodynamics Conference*, Chicago, IL, June 28 – July 1, 2010.

[6] Ansell, P.J., "Flight Envelope Protection Using Flap Hinge Moment Measurement," M.S. Thesis, University of Illinois at Urbana-Champaign, 2010.

[7] Lee, S., "Effect of Supercooled Large Droplet Icing on Airfoil Aerodynamics," Ph.D. Dissertation, Dept. of Aeronautical and Astronautical Engineering, Univ. of Illinois, Urbana, IL, 2001.

[8] Rae, W.H. and Pope, A., *Low-Speed Wind Tunnel Testing*, Wiley, New York, 1984, pp. 349-362, 449.

[9] Bush, R. H., 1988. "A Three Dimensional Zonal Navier-Stokes Code for Subsonic Through Hypersonic Propulsion Flowfields," AIAA Paper 88-2830.

[10] Bush, R.H., Power, G.D., & Towne, C.E., 1998. “WIND: The Production Flow Solver of NPARC Alliance”. AIAA Paper 98-0935.

[11] M. Mani, A. Cary, and S. V. Ramakrishnan. "A Structured and Hybrid-unstructured Grid Euler and Navier-Stokes Solver for General Geometry", AIAA Paper 2004-524.

[12] Spalart, P. R. and Allmaras, S. R., 1992. "A One-Equation Turbulence Model for Aerodynamic Flows", AIAA Paper 92-0439.

[13] Menter, F. R., 1993. "Zonal Two Equation k-omega Turbulence Models for Aerodynamic Flows", AIAA Paper 93-2906.

[14] Mani, M., Rider, B., Sclafani, T., Winkler, C., Vassberg, J., Dorgan, A., Cary, A., and Tinoco, E., “RANS Technology for Transonic Drag Prediction: A Boeing Perspective of the 4th Drag Prediction Workshop,” *28th AIAA Applied Aerodynamics Conference*, Chicago, IL, June 28 – July 1, 2010.

[15] Winkler, C., Dorgan, A., and Mani, M., “The Effect of Unstructured Grid Topology and Resolution on Simulations of Decaying Turbulence,” *27th Congress of the International Council of the Aeronautical Sciences (ICAS)*, paper number 682, Nice, France, 2010.

[16] Winkler, C. M., Dorgan, A. J., and Mani, M., “Scale Adaptive Simulations of Turbulent Flows on Unstructured Grids”, *29th AIAA Applied Aerodynamics Conference*, Honolulu, HI, June 27 – 30, 2011.